CrossMark

MRS Advances © 2017 Materials Research Society
DOI: 10.1557/adv.2017.154

Synthesis and Characterization of Nano-crystalline $La_2Zr_2O_7$ Film by Reactive Spray Deposition Technology for Application in Thermal Barrier Coatings

Yang Wang[1], Rishi Kumar[1], Justin Roller[2] and Radenka Maric[1]
[1] University of Connecticut, 97 North Eagleville Road, Storrs, CT 06269-3136
[2] FEI Company, 5350 NE Dawson Creek Drive, Hillsboro, OR 97124

Abstract

Lanthanum zirconate ($La_2Zr_2O_7$) nano-crystalline films with cubic structure have been successfully prepared by a facile synthesis approach called reactive spray deposition technology (RSDT). $La_2Zr_2O_7$ nanoparticles are produced by combusting a precursor solution of lanthanum acetylacetonate hydrate and zirconium acetylacetonate dissolved in an organic solvent mixture. The nanoparticles formed during the combustion process are directly deposited onto the substrate. The composition and microstructure of the as-deposited films are extensively characterized by X-ray diffraction (XRD), scanning electron microscope (SEM) and transmission electron microscope (TEM). The thermal diffusivities of the films are investigated by the means of laser flash method.

1. Introduction

Some gas turbines and diesel engines require thermal barrier coatings (TBCs) to protect the metallic components exposed in extreme high temperature operating environment [1]. With the thermal insulation from TBCs, the higher gas inlet temperatures that are needed to improve the efficiency of these engines are allowable, and the requirements for the onboard cooling system can be lowered [2] and [3]. Yttria-stabilized zirconia (YSZ) as a top-layer of TBC has been widely adopted in the industry. However, when operated at temperature above 1200 ˚C, the YSZ coating is subjected to cracking failure due to volume expansion associated with crystal phase transformation. In recent years, rare earth zirconates have been rigorously investigated and are found to have high phase stability, low thermal conductivity and high melting point which are ideal thermophysical properties for TBC applications [4] and [5]. Among them, lanthanum zirconate ($La_2Zr_2O_7$) with cubic pyrochlore structure is of special interest. $La_2Zr_2O_7$ is structured with six octahedral of ZrO_6 as the backbone and La^{3+} ions as the void filings. Since phase transformation does not easily occur with vacancies at the ion sites, this material remains phase stable up to its melting point of 2300 °C. Comparing to yttria-stabilized zirconia, $La_2Zr_2O_7$ possess a lower thermal conductivity (1.56 $W{\cdot}m^{-1}{\cdot}K^{-1}$ vs. 2.1-2.2 $W{\cdot}m^{-1}{\cdot}K^{-1}$) and less tendency to sintering so the integrity of the porous structure in the coating can be preserved.

Conventional synthesis methods, such as solid state reaction, co-precipitation, sol-gel and hydrothermal reaction, have been employed to produce $La_2Zr_2O_7$ powders with high crystallinity [6-10]. Air plasma spraying and electron beam physical vapor deposition techniques are used to prepare high quality $La_2Zr_2O_7$ films. However, these methods generally require either time-consuming processing steps or expensive equipment. Reactive spray deposition technology, a single-step flame based deposition method in open atmosphere and a member of the spray pyrolysis family, has been developed to prepare nanostructured

coatings in a rapid fashion and at a lower cost. The precursor materials (e.g. acetylacetonates, acetates, and nitrates) and organic solvents (e.g. methanol, acetic acid, xylene and toluene) used in the operation of RSDT are inexpensive and readily available. The synthesis and deposition of nanomaterials are combined into a one-step continuous process which is also scalable. In addition, since in-situ annealing can be provided by a blank high temperature xylene flame, no post-deposition thermal treatment is needed. Thus eliminating the use of an expensive furnace and reducing the total process time can be accomplished.

RSDT enables precise control of the physical properties of synthesized materials, such as surface morphology, particle size distribution, coating density and porosity. Upon combustion, the decomposition of precursor materials rapidly occurs in the high temperature flame, followed by phase transition to vapor and homogeneous reactions to generate metal oxides. The mechanisms of particle growth in the flame can be summarized in the order of nucleation, surface growth, cluster formation, coalescence, aggregation, and agglomeration. Continuous physical impingement of in-flight nanoparticles leads to the formation of a film on the targeted substrate. During the synthesis process, precursor solution feed rate and oxidant flow rate determine the core temperature of the flame and the length of the hot reaction zone, which are important processing parameters in terms of fine-tuning the crystallinity and size of the synthesized nanoparticles. The temperature of the substrate also has a direct impact on the particle size distribution and the rate of film growth.

In this study, nanostructured $La_2Zr_2O_7$ films are successfully prepared by RSDT for the first time. Its chemical composition and microstructure are thoroughly investigated by means of XRD, SEM and TEM. The thermal diffusivities of the synthesized material are evaluated with a laser flash instrument.

2. Experimental

2.1. Synthesis of $La_2Zr_2O_7$ nano-crystalline film

The synthesis of the $La_2Zr_2O_7$ films was accomplished solely by RSDT. The complete equipment setup and operational details of RSDT can be found elsewhere [11-14]. Lanthanum acetylacetonate hydrate (Sigma Aldrich) was heat-treated at 120 ˚C for 5 hours to remove physically absorbed water. The dried lanthanum acetylacetonate powder and zirconium acetylacetonate (Sigma Aldrich) powder were dissolved into 50:50 wt. % methanol/acetic acid (ACS reagent grade, Sigma Aldrich) solvent mixture. The final concentration of the precursor materials in the solution was 10 mM and the molar ratio between La and Zr was 1:1. To ensure complete dissolution and mixing, the solution was put into an ultrasonic water bath for 90 minutes and a clear solution with no visible particulates was obtained. The precursor solution was then transferred into a pressure vessel and liquefied propane free of sulfur (Airgas East Inc.) was added to constitute 16.5% of the total solution weight. The solution was then transferred into a high-pressure syringe-pump and fed to the atomization nozzle at a flow rate of 4 mL/min. The addition of liquid propane helped reduce the size of the droplets exiting the atomizing nozzle due to supercritical expansion. The temperature of the precursor solution was elevated to 50–60 ˚C via induction heating coil wired around the liquid feed tubing. The atomized precursor solution coming out of the nozzle was ignited to create a turbulent flame which was sustained by six methane–oxygen

pilot burners (flow rate at 0.55 L/min each) located near the nozzle. A stainless steel disc (2.54 cm in diameter, 210 μm in thickness) was securely mounted on a stainless steel substrate holder that was fixed onto a computer-controlled motion platform. A piece of zero-diffraction silicon was also mounted on the holder to collect product material for XRD analysis. A thermocouple was mounted at the back of the substrate to measure its temperature during deposition.

2.2. Physical Characterization

The crystal structure and phase purity of the as-prepared $La_2Zr_2O_7$ film was examined by means of X-ray diffraction (XRD) using a Bruker D-8 advance diffractometer operated at 40 kV and 40 mA with Cu Kα radiation (λ= 1.5406 Å). FEI Quanta 250 FEG SEM with a field emission source was employed to characterize the surface microstructure of the $La_2Zr_2O_7$ film. The imaging was accomplished with Everhart-Thornley SE (secondary electron) detector operating at an electron accelerating voltage of 10 kV and sample height of 10 mm. FEI Metrios TEM/STEM system operating at an electron accelerating voltage of 200 kV with bright field and dark field detectors was employed to observe the particle morphology and size distribution of the $La_2Zr_2O_7$ nanoparticles. The $La_2Zr_2O_7$ film was scrapped off from the silicon substrate into a glass vial and small amount of ethanol was added. The vial was then put in water bath sonicator for 20 minutes in order to obtain homogenous suspension. To prepare TEM samples, few drops of the suspension was applied onto 300 mesh thin carbon film coated Cu grids (Ted Pella Inc.) which were dried in air overnight.

Thermogravimetric (TG) and differential scanning calorimetry analysis (DSC) were performed in nitrogen with Netzsch STA 449 F3 Jupiter Simultaneous Thermal Analyzer at a heating rate of 10 K min^{-1}. Powders of precursor materials were loaded in alumina crucible cups as sample holders. A laser flash apparatus (Netzsch LFA 457 MicroFlash) was employed to measure the thermal diffusivities of the as-prepared $La_2Zr_2O_7$ film on stainless steel substrate, as a function of temperature between 25 ˚C and 1000 ˚C. Before loading the sample into the instrument, a thin layer of graphite was applied to the front and back sides of the sample in order to avoid direct transmission of laser beam through the sample.

3. Results and discussion

3.1. Synthesis of $La_2Zr_2O_7$ thin film

3.1.1. Thermal analysis of precursor materials

The TG–DSC results of metal acetylacetonate precursor materials are shown in Figure 1. It shows an endothermic peak in the DSC curve and a weight loss in the TG curve between 100 and 200 °C for both precursor materials. The desorption of physically absorbed water can be attributed to this change. The weight of the acetylacetonates drops sharply as the temperature increases from 200 °C to 500 °C. At about 500 °C, an exothermic peak in the DSC curve of Figure 1a can be observed, which can attributed to the decomposition of lanthanum acetylacetonate. From 350°C to 560°C, a broad exothermic peak centered at 500°C in the DSC curve of Figure 1b is present, which can be attributed to the decomposition of zirconium acetylacetonate. Hence, both precursor materials exhibit comparable decomposition temperatures which are deemed to be beneficial for the formation of stochiometric $La_2Zr_2O_7$ solid solution.

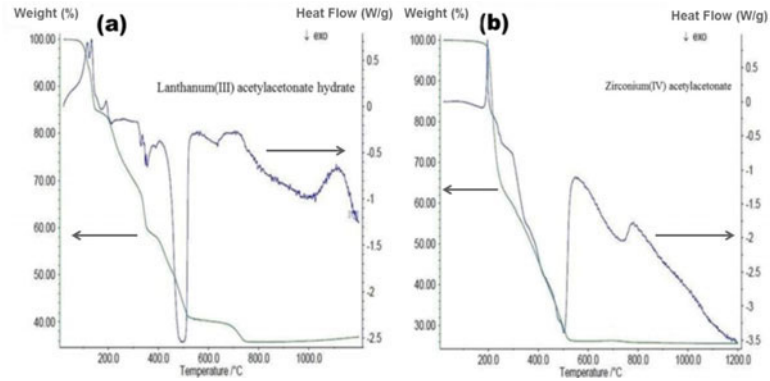

Figure 1. TG–DSC curves of precursor materials

3.1.2. XRD studies

XRD pattern of the $La_2Zr_2O_7$ film prepared by RSDT is shown in Figure 2 to demonstrate the crystalline phase. Two types of structures, pyrochlore and fluorite of $La_2Zr_2O_7$, have been reported [15]. The pyrochlore structure has a close resemblance to the fluorite structure in terms of the XRD peaks. With the confirmation of standard XRD profile of $La_2Zr_2O_7$ (JCPDS Card No. 73-0444), it is confirmed that pure phase $La_2Zr_2O_7$ material with cubic pyrochlore structure has formed. The main peak [222] is the highest in intensity, indicating that it is the most favored plane during the formation of $La_2Zr_2O_7$ in the hot reactive flame.

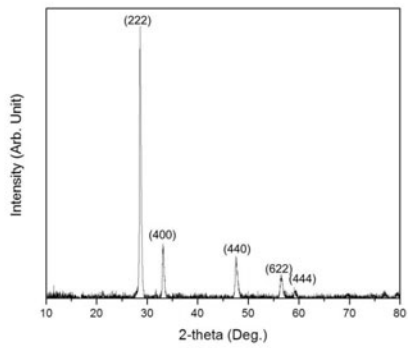

Figure 2. XRD pattern of as-prepared $La_2Zr_2O_7$ film on zero-diffraction silicon substrate.

3.2. Physical characterization

3.2.1. SEM

The surface morphology of the as-prepared $La_2Zr_2O_7$ film is shown in Figure 3a. It is

observed that the aggregates of $La_2Zr_2O_7$ are uniformly distributed on the substrate. This is likely due to the fact that the entire flame reaction zone is turbulent and the mixing of particles is efficient. Figure 3b clearly shows the cauliflower-like structure of as-synthesized $La_2Zr_2O_7$ material and the high porosity present in the film.

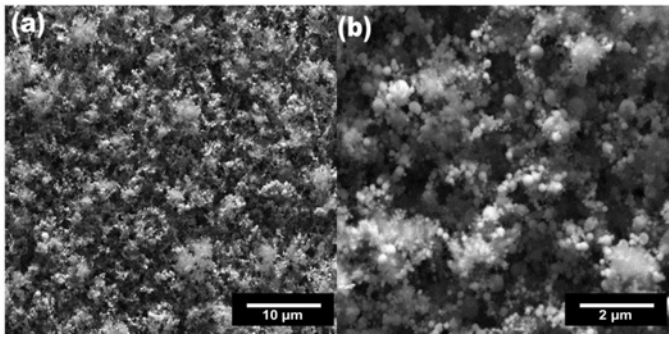

Figure 3. Surface morphologies of nanostructured $La_2Zr_2O_7$ film deposited on stainless steel substrate.

3.2.2. TEM

The detailed morphologies of the $La_2Zr_2O_7$ nanoparticles were characterized by TEM. Figure 4a and figure 4b show that the majority of $La_2Zr_2O_7$ nanoparticles synthesized by RSDT are spherical. Mono-dispersed sheet particles can be observed in Figure 4c, demonstrating high crystallinity. Diffraction pattern acquired from a selected area of representative particles (Figure 4d & 4e) demonstrates that the $La_2Zr_2O_7$ nanoparticles are polycrystalline. The obtained d-spacings closely match with the corresponding diffraction peaks of pyrochlore $La_2Zr_2O_7$ with cubic structure.

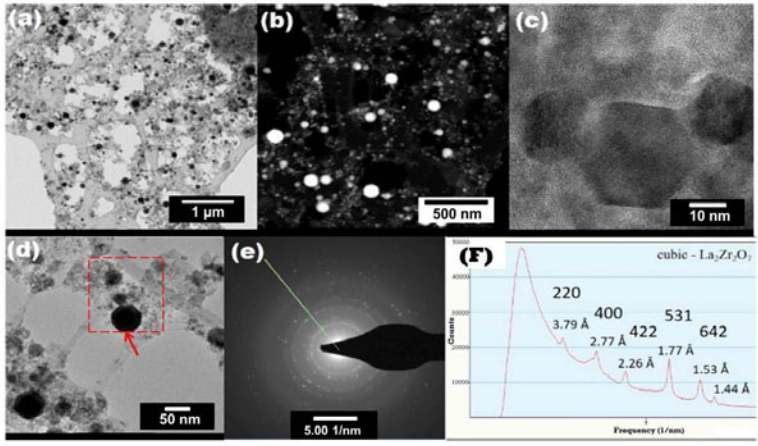

Figure 4. TEM images of $La_2Zr_2O_7$ nanoparticles synthesized by RSDT: (a) an overview of the morphology in bright field, (b) an overview of the morphology in dark field, (c) high-resolution TEM image, (d) high-magnification TEM image (the red arrow indicates the focused area of electron beam to acquire the diffraction pattern) , (e) diffraction pattern, (f) measured d-spacings from the diffraction rings.

3.3. Thermophysical property

Thermal diffusivity data of the $La_2Zr_2O_7$ film acquired by laser flash method is shown in Figure 5. It can be observed that thermal diffusivities exhibit a decreasing trend with increasing temperatures in the range between room temperature and 1000 °C. This behavior is consistent with polycrystalline $La_2Zr_2O_7$ materials and suggests the mechanism of heat transfer as phonon conduction. This can be explained by the fact, with increasing temperature, phonons start to vibrate at higher frequency thereby increasing the probability of interacting with each other, also known as phonon-phonon scattering [16]. The measured thermal diffusivities of the nano-crystalline $La_2Zr_2O_7$ film in this work are considerably lower than those reported in the literature [17-20]. However, the underlying mechanisms that lead to such decrease in thermal diffusivities are unclear at this point. Further in-depth investigation of the influences of the crystal structure (i.e. preferred crystal orientation) and the morphologies (i.e. size and shape) of the synthesized $La_2Zr_2O_7$ particles on the thermal diffusivity of the film will be conducted.

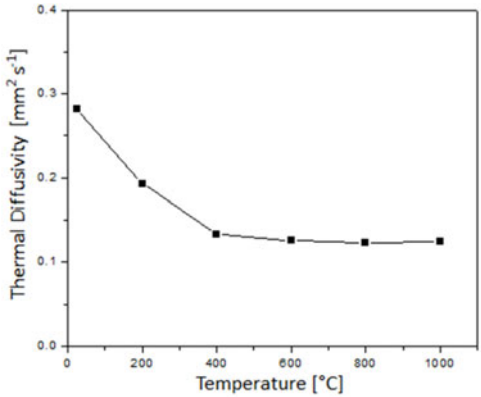

Figure 5. Thermal diffusivities of the $La_2Zr_2O_7$ film as a function of temperatures.

4. Conclusion

The nano-crystalline $La_2Zr_2O_7$ films are successfully prepared by RSDT. The synthesis and deposition of $La_2Zr_2O_7$ films are combined into a one-step continuous process which is also scalable. It offers a convenient and low-cost alternative synthesis route to current state of art methods. SEM and TEM analysis indicates that the synthesized $La_2Zr_2O_7$ material is polycrystalline and composed of uniformly distributed aggregates. The as-prepared $La_2Zr_2O_7$ film demonstrates significantly lower thermal diffusivities comparing to those reported in the literature, which are ideal thermophysical property for application in thermal barrier coatings.

Further investigation will focus on the underlying mechanisms that lead to the decrease in thermal diffusivities.

Acknowledgments

The authors gratefully acknowledge the School of Engineering at University of Connecticut for the financial support and the Center for Cleaning Energy Engineering at University of Connecticut for the facility use.

References:

1. R. Cremer, M. Witthaut, K. Reichert, M. Schierling, D. Neuschuetz, Surf. Coat. Technol. 108–109, 48–58 (1998).
2. A.G. Evans, D.R. Clarke, C.G. Levi, J. Eur. Ceram. Soc. 28, 1405–1419 (2008).
3. J.W.P. Hsu, Z.R. Tian, N.C. Simmons, C.M. Matzke, J.A. Voigt, J. Liu, Nano Lett. 5, 83 (2005).
4. J. Yang, D. Li, X. Wang, X.J. Yang, L.D. Lu, J. Solid State Chem. 165, 193 (2002).
5. H.M. Zhou, D.Q. Yi, Z.M. Yu, L.R. Xiao, J. Alloys Compd. 438, 217 (2007).
6. K. Koteswara Rao, M. Taqveem Banu, G.Y.S.K. Vithal, K. Swamy, R. Kumar, Mater. Lett. 54, 205 (2002).
7. Tong, Junwu Zhu, Lude Lu, Xin Wang, Xujie Yang, J. Alloys Compd. 465, 280 (2008).
8. Y. Matsumura, M. Yoshinaka, K. Hirota, O. Yamaguchi, Solid State Commun. 104, 341 (1997).
9. Yuping Tong, Yanping Wang, Zongxue Yu, Xin Wang, Xujie Yang, Lude Lu, Mater. Lett. 62, 889 (2008).
10. D. Chen, R. Xu, Mater. Res. Bull. 33, 409 (1998).
11. J.M. Roller, M. Josefina Arellano-Jiménez, H. Yu, R. Jain, C. Barry Carter, R. Maric, Electrochim. Acta. 107, 632–655 (2013).
12. J.M. Roller, M. J. Jiménez, R. Jain, H. Yu, R. Maric, C. B. Carter, Processing, ECS Trans. 45, 97-106 (2013).
13. R. Maric, J. Roller, R. Neagu, J. Therm. Spray Technol. 20, 696–718 (2011).
14. R. Maric, TPK. Vanderhoek, J.M. Roller, US Patent App. 370 (2008).
15. X.Q. Cao, R. Vassen, W. Fischer, F. Tietz, W. Jungen, D. Stoever, Adv. Mater. 15, 1438 (2003).
16. X. Wang et al., Applied Surface Science 257, 8945– 8949 (2011).
17. H.M. Zhou, D.Q. Yi, Z.M. Yu, L.R. Xiao, J. Alloys Compd, 438, 217-221 (2007).
18. H. Lehmann, D. Pitzer, G. Pracht, R. Vassen, D. Stover, J. Am. Ceram. Soc. 86, 1338-1344 (2003).
19. H.F. Chen, Y.F. Gao, Y. Liu, H.J. Luo, J. Alloys Compd 480.2, 843-848 (2009).
20. H Chen, Y Gao, S Tao, Y Liu, H Luo, J. Alloys Compd 486.2, 843-848 (2009).